Peg-on-Hole: A Model Based Solution to Peg and Hole Alignment

H. Bruyninckx, S. Dutré and J. De Schutter
Katholieke Universiteit Leuven
Department of Mechanical Engineering, Division PMA
Celestijnenlaan 300B, B-3001 Heverlee, Belgium
e-mail: Herman.Bruyninckx@mech.kuleuven.ac.be

Abstract

Most of the literature on the classical "peg-in-hole" problem concentrates on the insertion phase. In unstructured environments, however, the preceding phases of finding the hole and aligning the axes of peg and hole are equally important. This text describes how to model the "peg-on-hole" contact situation, and how to specify the alignment motion for arbitrarily large alignment errors between the axes of peg and hole. The results are given for any radius of peg and hole. They are applied in a real world experiment, in which also some uncertainties in the location of the hole are resolved on line by active force sensing.

1 Introduction

Insertion operations are an important aspect of assembly. Tight tolerances between both objects involved in the insertion, as well as positioning inaccuracies, require some level of on line adaptation of the programmed trajectories. This adaptation is implemented passively (by means of compliance) or actively (by means of force control). Since the seminal work of Whitney [6] and his co-workers at Draper Lab, the cylindrical *peg-in-hole* problem is well understood, and robust solutions, both active and passive, have emerged. This research and that of its followers ([3, 4, 5]) concentrate on: 1) how to avoid wedging and jamming; 2) how to model and recognize (by means of force-torque sensing) all possible contact situations during the insertion; and 3) cylindrical and rectangular pegs. However, some important aspects for a "complete" peg-in-hole in an unstructured environment are neglected:

- A complete task consists of: 0) locate the peg with respect to the robot, and resolve the uncertainties in the peg's geometry; 1) approach the hole's environment; 2) locate the exact position of the hole in this environment; 3) align the peg on the hole; 4) insert. The robotics literature concentrates on point 4) and on *control*; this article is about points 2) and 3): how to find the hole; how to model the contact situation between a badly aligned peg and the hole; and how to specify the nominal motion to decrease the alignment error.
- A good pre-insertion alignment of peg and hole avoids wedging and jamming at entrance.
- A better nominal motion specification increases the "quality" of the task execution: a smaller pre-insertion misalignment results in smaller contact forces and allows a higher insertion speed.

Consider the contact situation between a substantially misaligned peg and hole, Fig. 1. This three-point contact is more stable and is obtained more reliably during the approach than with a quasi-aligned peg. Starting the insertion task from this initial position would lead to immediate failure. To resolve the misalignment, the peg has to be rotated until its axis is parallel to the hole's axis. However, the instantaneous rotation axis changes during the motion (with respect to the hole as well as to the peg), in a nonlinear way, especially if the contact between peg and hole is to be maintained. Hence, the specification of this alignment motion has to be deduced from a *model*.

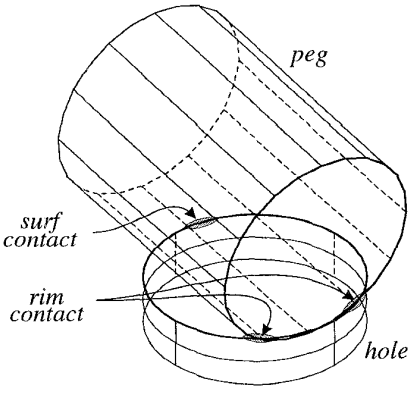

Figure 1: *Peg-on-hole*: a large misalignment between the axes of peg and hole requires a time varying motion specification to decrease the alignment error without breaking the contacts.

Section 2 states the *peg-on-hole* problem, and gives two modelling approaches: 1) a kinematic model in terms of *virtual contact manipulators*, and 2) an *ad*

IEEE International Conference on Robotics and Automation
0-7803-1965-6/95 $4.00 ©1995 IEEE

hoc geometric model, which strongly simplifies the general kinematic model by exploiting some task-specific geometric relationships. Section 3 uses these models to generate the nominal alignment motion. The results are independent of the size of peg and hole. The last Section discusses the experimental results of a real world execution of the task.

2 Modelling

The three-point contact of Fig. 1 is the *most stable* and the *least uncertain* contact situation between the cylindrical peg and the hole, unless the peg is already partially inserted. This is because:

- The motion freedom of the peg is constrained by three distinct contacts, Fig. 1:

  1. *surf*: the contact between the outer surface of the peg and the rim of the hole.
  2. *rim1* and *rim2*: the two contacts between the bottom rim of the peg and the rim of the hole. These two contacts are positioned symmetrically with respect to the plane through the peg's axis and through *surf*.

  Each contact eliminates one degree of freedom. Hence the total number of degrees of freedom of the peg with respect to the hole is three, as well as the dimension of the space spanned by the normal vectors at each of the three contacts, the so-called *wrench* space. This also means that the uncertainty in the relative position between the peg and the hole is smaller than with only one or two contacts.

- The stability of the contact situation is proportional to the area of the triangle formed by the three points of support on the top rim of the hole. This area is function of the alignment error. This alignment error α is the angle between the axis of the peg and the axis of the hole. The larger the surface, the more stable the contact situation. Figure 2 shows this support triangle for different alignment errors α. Its area is maximal for an alignment error of 1.231 *rad*.

The following subsections describe two different modelling approaches of this three-point contact: the first one is the most general approach, and is based on *virtual manipulators* to numerically model the motion freedom in each contact, [1]; the second one is an *ad hoc* geometric approach, which results in a closed form solution. Hence, it is more efficient but less flexible than the kinematic approach.

2.1 Kinematic model

The presented kinematic model of the peg-on-hole problem is an application of the general modelling theory for constrained manipulation as presented by the authors in [1]. Each of the three point contacts is modelled by means of a five degrees-of-freedom virtual manipulator, Figs. 3 and 4. These manipulators form three parallel connections between the hole and the peg, and constrain the peg's motion freedom in the same way as the contacts. More precisely, they

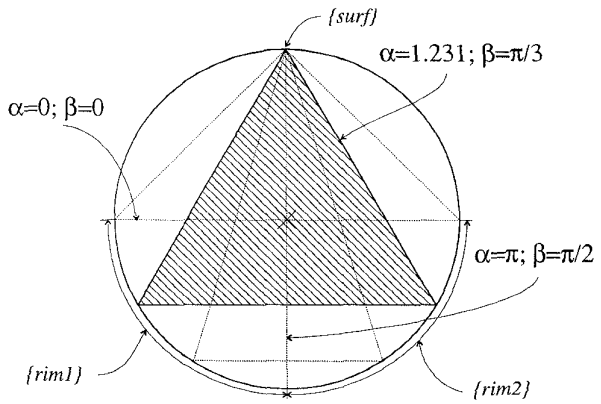

Figure 2: Triangle formed by the three points of support on the top rim of the hole, for different alignment errors α. The contact situation is most stable at an alignment error of 1.231 *rad*. This situation corresponds to the shaded support triangle, which is equilateral, i.e., the angle $\beta = \pi/3$ *rad*.

constrain the *reciprocal* motion freedom of the peg in the same way as the contacts. This means that the motions of the peg which *maintain the three contacts* are exactly the motions allowed by the kinematic chain formed by the three virtual manipulators.

Given the alignment error α between the axes of peg and hole, the kinematics of each of these manipulators is completely determined. Individually, each manipulator allows five degrees-of-freedom, but all three in parallel allow only three degrees-of-freedom. At least, for the non-degenerated positions, i.e., the misalignment is different from 0 or 90 degrees. A basis for the instantaneous motion freedom of the peg with respect to the hole has three independent components; one possible representation for this basis is stated in terms of the following motions:

Slip : rotation of the peg about its own axis.

Slide : rotation of the peg about the hole's axis.

Align : rotation of the peg about the tangent to the hole's rim, at the contact point.

As for "normal" manipulators, the *Jacobian* of each virtual manipulator gives the relation between its "joint" velocities and the velocity of its "end effector," i.e., the relative velocity of the peg with respect to the hole. It is a tedious but straightforward job to calculate these three Jacobians from the geometry of the task, as defined by Fig. 5, see [1]. Each Jacobian is a 6×5 matrix, modelling the five degrees-of-freedom allowed in each contact. The three degrees-of-freedom of the combined constraint are found from the following *velocity closure* equations:

$$\begin{bmatrix} \dot{p} \\ \omega \end{bmatrix} = \boldsymbol{J}^s \dot{\boldsymbol{q}}^s = \boldsymbol{J}^1 \dot{\boldsymbol{q}}^1 = \boldsymbol{J}^2 \dot{\boldsymbol{q}}^2. \qquad (1)$$

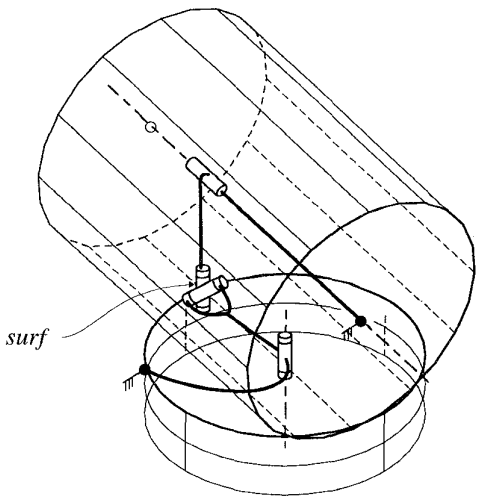

Figure 3: *"Surf" contact.* Its kinematic model consists of a five degrees-of-freedom manipulator: one cylindrical joint (two degrees-of-freedom) along the peg's axis, and revolute joints along the hole's axis, along the tangent to the hole's rim at the contact point, and along the contact normal.

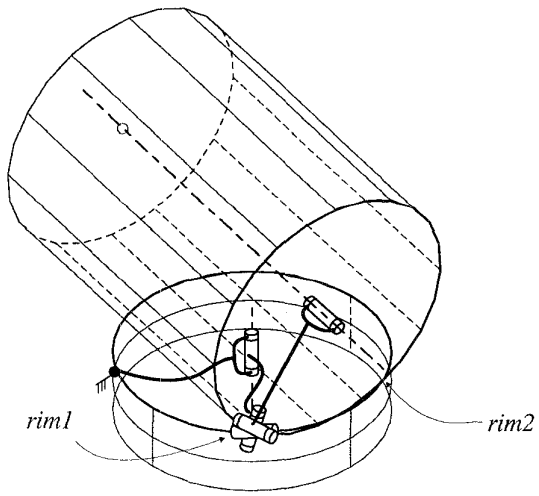

Figure 4: *"Rim" contacts.* Their kinematic models consist of five degrees-of-freedom manipulators: revolute joints along the axes of peg and hole, along the tangents to the rims of hole and peg at the contact point, and finally along the contact normal. (Only the kinematic chain of *rim1* is shown; that of *rim2* is completely similar.)

$\dot{\boldsymbol{p}}$ is the translational velocity of the peg; $\boldsymbol{\omega}$ is its angular velocity. $\boldsymbol{J}^s$ is the Jacobian of the *surf* contact, and $\boldsymbol{J}^1$ and $\boldsymbol{J}^2$ are the Jacobians of the *rim1* and *rim2* contacts. The $\dot{\boldsymbol{q}}^i$ are the joint velocities of the corresponding virtual manipulators. It is straightforward to check that **Slip**, **Slide** and **Align** are the three degrees-of-freedom obeying all constraints imposed by the velocity closure equations of (1).

From the knowledge of all individual Jacobians, the *evolution* of the kinematic model is calculated numerically: the speed of each joint in the kinematic structure determines how the structure changes over time.

2.2 Geometric model

For cylindrical pegs and holes, the general kinematic description of the previous paragraphs can be simplified to a closed form solution. This describes the relationships between, on the one hand, the coordinates of each contact point with respect to both peg and hole, and, on the other hand, the alignment error.

The *surf* contact point lies on the outer surface of the peg, as well as on the top rim of the hole. Hence, it has the following coordinates with respect to the reference frames at the peg's bottom ($\{peg\}$) and the hole's top ($\{hole\}$):

$$\begin{aligned} \boldsymbol{p}_{surf}^{peg} &= [0\ h\ -r]^T, \\ \boldsymbol{p}_{surf}^{hole} &= [0\ 0\ -r]^T, \end{aligned} \tag{2}$$

with r the radius of the peg, h the height of the contact point as measured along the peg's axis.

Both *rim* contact points lie on the peg's bottom rim, as well as on the hole's top rim. The angle β between the X axis and the radius through the contact point is the same for both peg and hole, since it spans the same arc on two circles with the same radius. This gives:

$$\begin{aligned} \boldsymbol{p}_{rim1}^{peg} &= [-rc_\beta\ 0\ -rs_\beta]^T, \\ \boldsymbol{p}_{rim1}^{hole} &= [-rc_\beta\ 0\ rs_\beta]^T, \\ \boldsymbol{p}_{rim2}^{peg} &= [rc_\beta\ 0\ -rs_\beta]^T, \\ \boldsymbol{p}_{rim2}^{hole} &= [rc_\beta\ 0\ rs_\beta]^T, \end{aligned} \tag{3}$$

with $c_\beta = \cos(\beta)$ and $s_\beta = \sin(\beta)$. If α is the alignment error (i.e., the angle between the Z axes of the reference frames $\{peg\}$ and $\{hole\}$), the homogeneous transformation matrix ${}^{peg}_{hole}\boldsymbol{T}$ from the peg's reference frame $\{peg\}$ to the hole's reference frame $\{hole\}$ is given by:

$${}^{peg}_{hole}\boldsymbol{T} = \begin{bmatrix} 1 & 0 & 0 & 0 \\ 0 & c_\alpha & s_\alpha & p_y \\ 0 & -s_\alpha & c_\alpha & p_z \\ 0 & 0 & 0 & 1 \end{bmatrix}, \tag{4}$$

with $c_\alpha = cos(\alpha), s_\alpha = sin(\alpha)$, and $[0\ p_y\ p_z]^T$ the coordinates of the origin of $\{peg\}$ with respect to $\{hole\}$.

The relations between the parameters α, β, h, r, p_y and p_z are easily derived from Eqs. (2)-(4):

$$\begin{aligned} \boldsymbol{p}_{surf}^{hole} &= {}^{peg}_{hole}\boldsymbol{T}\ \boldsymbol{p}_{surf}^{peg}, \\ \boldsymbol{p}_{rim}^{hole} &= {}^{peg}_{hole}\boldsymbol{T}\ \boldsymbol{p}_{rim}^{peg}, \end{aligned} \tag{5}$$

which result in:

$$p_y = rs_\alpha \frac{1 - c_\alpha}{1 + c_\alpha}, \tag{6}$$

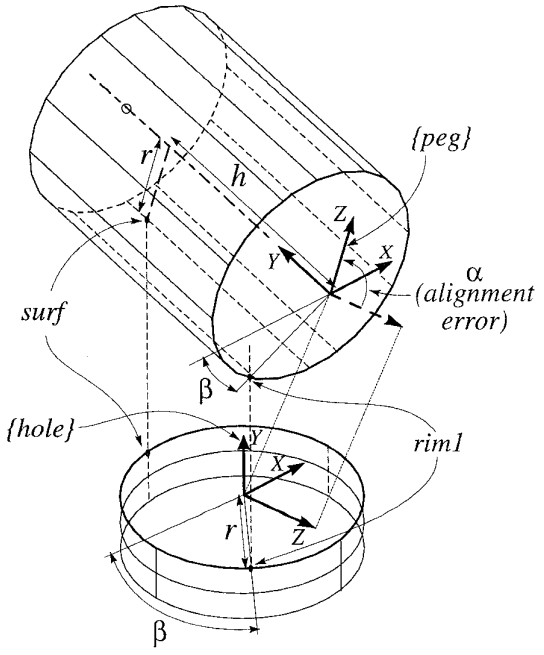

Figure 5: *Peg-on-hole, expanded geometric model.*

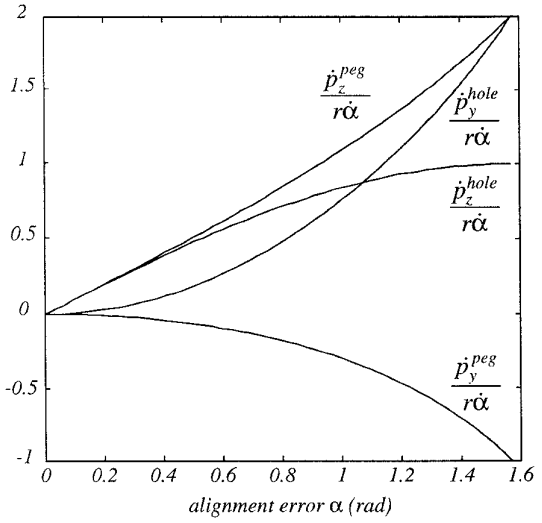

Figure 6: *Velocity profiles.* The instantaneous velocities needed to align the peg on the hole are given as functions of the alignment error α. The profiles are dimensionless, since they are given for a unit radius r and a unit angular alignment speed $\dot{\alpha}$. The reference frames are as in Fig. 5.

$$\begin{aligned} p_z &= r(1-c_\alpha), \\ \beta &= \arcsin(\frac{1-c_\alpha}{1+c_\alpha}), \\ \alpha &= 2\arctan(h/2r), \\ h &= 2r\tan(\alpha/2). \end{aligned} \tag{7}$$

The time derivatives of Eqs. (6)-(7) give the velocities of the peg's reference frame with respect to the hole, as functions of the angular alignment velocity $\dot{\alpha}$:

$$\begin{aligned} \dot{p}_y &= r\frac{(2+c_\alpha)(1-c_\alpha)}{1+c_\alpha}\dot{\alpha}, \\ \dot{p}_z &= rs_\alpha\dot{\alpha}. \end{aligned} \tag{8}$$

Since the peg is the manipulated object, it is more interesting to specify its motion with respect to its own reference frame $\{peg\}$. The transformation of Eqs. (8) to $\{peg\}$ gives:

$$\begin{aligned} \dot{p}_y^{peg} &= c_\alpha\dot{p}_y - s_\alpha\dot{p}_z = r\frac{c_\alpha-1}{c_\alpha+1}\dot{\alpha}, \\ \dot{p}_z^{peg} &= s_\alpha\dot{p}_y + c_\alpha\dot{p}_z = \frac{2rs_\alpha}{c_\alpha+1}\dot{\alpha}. \end{aligned} \tag{9}$$

3 Task specification

3.1 Desired motion

The previous Section defined the three degrees-of-freedom of the peg-on-hole problem as **Slip, Slide** and **Align**. In the kinematic model these degrees-of-freedom correspond to motion of three particular joints: the revolute joints along the axes of the peg and the hole (**Slip** and **Slide**), and the revolute joint along the tangent to the hole's rim at the *surf* contact point (**Align**). Generating a motion of the peg corresponds to assigning desired speeds to each of these *driving joints*. In the sequel, only the alignment motion is considered.

Two natural ways to specify the alignment motion are: 1) to specify the time rate of the **Align** joint, $\dot{\alpha}$; or, 2) to specify the time rate of the position of the *surf* contact along the surface of the peg, $\dot{h}$. Both drive the same degree-of-freedom, and hence they are connected by a (non-linear) one-to-one relationship:

$$\dot{\alpha} = \frac{\dot{h}}{r(1+(h/2r)^2)}. \tag{10}$$

Figure 6 shows the velocity profiles (i.e., translational velocities of the peg's reference frame in the Y and Z directions of $\{peg\}$ and $\{hole\}$) resulting from a constant angular alignment speed $\dot{\alpha}$ as calculated from Eqs. (8)-(9). The profiles have been made dimensionless through scaling by the radius r and the alignment speed $\dot{\alpha}$. Hence, the results can be used to generate the peg trajectory for any radius and alignment velocity. It has been checked by the authors that the velocity profiles of Fig. 6 perfectly agree with those generated by the velocity closure equations of the kinematic approach.

3.2 Desired reaction forces

The kinematic or geometric models not only generate the nominal motions of the peg with respect to the hole, but they can also describe which ideal reaction

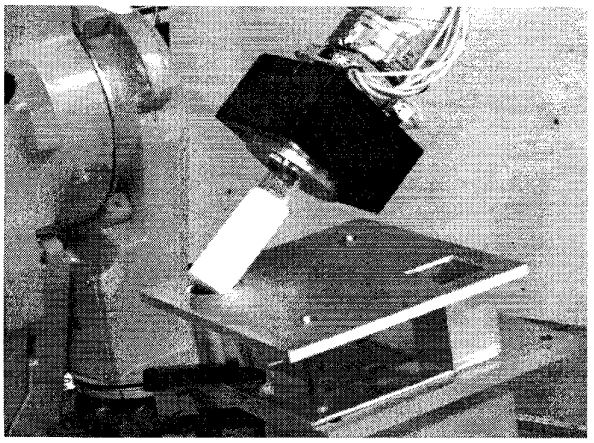

Figure 7: *Experimental setup :* the robot's end effector holds a flexible force sensor to which a peg (with radius $r = 25mm$) is connected.

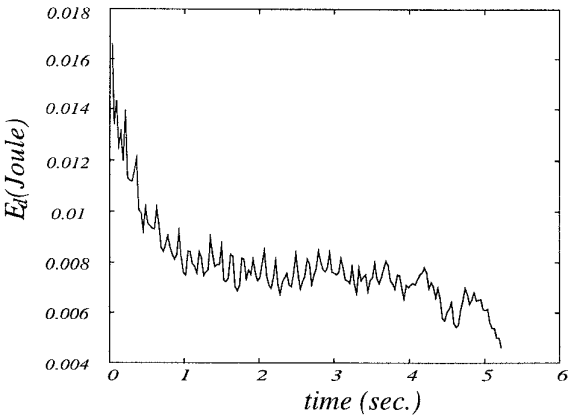

Figure 8: *Deformation energy of the compliant structure during alignment.* The initial alignment error was about 60 *deg*, the angular alignment speed $\dot{\alpha} = 0.2\ rad/sec.$

forces are possible. It is indeed straightforward to calculate the directions of the contact normals at each of the three contact points:

surf : the normal direction is the direction of the Z axis of $\{peg\}$.

rim : take the vector product of the tangents to peg and hole at the contact point; these tangent directions are obtained as the derivative with respect to β of Eqs. (3).

Then, all ideal reaction forces in that contact point lie along this normal direction. Hence, all possible reaction forces for the total peg-on-hole constraint are linear combinations of the contact forces at the individual contact points.

4 Experiment

The peg-on-hole task applies to assembly tasks in a poorly structured environment (for example, assembly in space or in a nuclear environment). A complete peg-in-hole task has been performed with a real robot. Its end effector holds a compliant six component force sensor to which a pen (with radius $r = 25mm$) is connected (see Fig. 7). This sensor measures deformations rather than strains. Hence, it knows the exact position and velocity of the peg. Forces are obtained by multiplying the deformations with the stiffness matrix of the compliant structure. This stiffness matrix with respect to the centre of compliance, $[k_x\ k_y\ k_z\ k_{xx}\ k_{yy}\ k_{zz}]^T$, is approximately [45 60 45 N/mm 175000 225000 175000 Nmm/rad]^T.

The hole is located in a horizontal plane below the peg, and its exact position is only approximately known. The task is executed with a *task frame* based programming interface, [2], extended with feedforward capability to generate the model based peg-on-hole alignment motion. The task strategy is as follows:

1. The peg is rotated about X of $\{peg\}$ over a known alignment error α of about 1 *rad*, which approaches the best value 1.231 *rad* without danger of touching the plane of the hole with the force sensor.
2. The peg is moved downwards until it contacts the plane of the hole. The contact point is such that the tip of the peg now points towards the expected location of the hole.
3. The force controller pushes the peg forward over the plane, in the direction in which the hole is expected (i.e., the specification for the force controller is: a force ($30N$) in the Y direction of $\{peg\}$, no forces in X and Z, and no torques). It stops when it encounters a reaction force in the direction of motion which is significantly larger than the friction force (i.e., the termination condition is: stop when the force in the Y direction exceeds $28N$). Since the peg has previously been tilted, this termination condition guarantees that the peg has "fallen" into the hole. If the direction of search is too uncertain, other high level search strategies must be used.
4. The desired three-contact configuration is established by slightly pushing the peg into the hole, i.e., a force in Y and Z, no force in X.
5. Now, the alignment motion is executed, with the velocity profiles $\dot{p}_y^{peg}$ and $\dot{p}_z^{peg}$ of Fig. 6. At each time step the alignment error is estimated taking into account the measured deformations. This part of the task is performed without force control; the small inaccuracies due to the discrepancies between the model and reality are taken up by the compliant sensor structure. Figure 8 shows the deformation energy stored in the flexible structure during this alignment:

$$E_d = k_y d_y^2 + k_z d_z^2 + k_{xx} \delta_x^2, \qquad (11)$$

with d_y and d_z the translational deformations (mm) in Y and Z, and δ_x the angular deformation (rad) about X with respect to a frame at the centre of compliance.

The alignment motion is programmed with a *constant* angular velocity $\dot{\alpha}$. Hence, an acceleration jump occurs in the motion of the robot. Due to inertial effects, the peg does not immediately follow the motion of the robot end effector, and hence the deformation energy shows a peak at the start of the motion. After this inertial transition phase, the deformation energy remains more or less constant, indicating that the discrepancies between model and reality remain small. Visual inspection reveals also that the contacts are maintained.

6. After the motion, the peg is so well aligned with the hole, that an insertion without active force control is possible (clearance of the peg: $\pm.25mm$).

The success rate of this experiment is high, once the three points contact is reached which proves the accuracy of the model.

5 Conclusions

This paper introduced "peg-on-hole" as one of the phases of a complete peg-in-hole assembly task in an unstructured environment. Its main characteristic is the non-linear time variance of the instantaneous motion freedom of the peg with respect to the hole. Two approaches are described to model this motion freedom: the first approach models each contact as a five degrees-of-freedom virtual manipulator; the second approach uses the particular geometric properties of the peg-on-hole problem to derive an analytical solution. The former approach is easier to extend to other contact situations, while the latter is more efficient.

Two important practical problems need special attention:

1. The estimation of the alignment error between the axes of peg and hole at the start of the peg-on-hole motion.

2. The development of a strategy to reliably locate the position of the hole when the environment is uncertain.

The theoretical developments have been successfully tested on a real world experiment. This experiment includes finding the hole in a plane when its location is uncertain to within about the radius of the peg. The alignment of peg and hole, and the subsequent insertion, are performed without active force control, but the desired contacts are never broken and the deformation energy of the compliance doesn't increase.

Acknowledgement

H. Bruyninckx is Post-Doctoral Researcher of the N.F.W.O. (the Belgian National Fund for Scientific Research). This work was also sponsored by the *SECOND* project of the European Community (ESPRIT Basic Research Action 6769), and the Belgian Programme on Interuniversity Attraction poles initiated by the Belgian State – Prime Minister's Office – Science Policy Programming (IUAP-50). The scientific responsibility is assumed by its authors. Thanks to Adhi Sudadi and Sabine Demey for Fig. 7.

References

[1] Bruyninckx, H, Demey, S., Dutré, S. and De Schutter, J., *Kinematic Models for Model Based Compliant Motion in the Presence of Uncertainty*, accepted for publication in The International Journal of Robotics Research, 1995.

[2] De Schutter, J. and Van Brussel, H., *Compliant Robot Motion I. A Formalism for Specifying Compliant Motion Tasks*, International Journal of Robotics Research, Vol. 7, No. 4, pp.3–17, 1988.

[3] McCarragher, B. J. and Asada, H., *Qualitative Template Matching Using Dynamic Process Models for State Transition Recognition of Robotic Assembly*, Journal Dynamic Systems, Measurement and Control, Vol. 115, pp. 261–269, 1993.

[4] Puente, E. A., Balaguer, C. and Barrientos, A., *Force-Torque Sensor-Based strategy for Precise Assembly Using a SCARA Robot*, Robotics and Autonomous Systems, Vol. 8, pp. 203–212, 1991.

[5] Sturges, R. H. Jr., *A Three-Dimensional Assembly Task Quantification with Application to Machine Dexterity*, International Journal of Robotics Research, Vol. 7, No. 4, pp. 34–78.

[6] Whitney, D.E., *Quasi-Static Assembly of Compliantly Supported Rigid Parts*, Journal Dynamic Systems, Measurement and Control, Vol. 104, pp. 65–77, 1982.

[7] Xu, Y. and Paul, R. P., *A Robot Compliant Wrist System for Automated Assembly*, Proceedings of the IEEE International Conference on Robotics and Automation, pp. 1750-1755, 1990.